DOI: 10.1002/ejic.200600104

Correlation Between Structure and Magnetic and Magnetotransport Properties of $La_{0.7}Pb_{0.3}(Mn_{1-x}Co_x)O_3$ ($0.1 \leq x \leq 0.3$) CMR Manganites

Alazne Peña,[a] Jon Gutiérrez,*[b] Izaskun Gil de Muro,[a] Javier Campo,[c][‡] Jose Manuel Barandiarán,[b] and Teófilo Rojo[a]

Keywords: Manganites / Crystal structure / Magnetic properties / Magnetoresistance / Metal–insulator transition / Perovskite phases

Structural and magnetic properties of $La_{0.7}Pb_{0.3}(Mn_{1-x}Co_x)O_3$ ($0.1 \leq x \leq 0.3$) manganites are reported. Samples were fabricated by the sol-gel low temperature method. At room temperature, the first structural characterisation of all phases gave as a result the rhombohedral space group ($R\bar{3}c$). All compositions show ferromagnetic behaviour and magnetoresistance. The measured low-temperature magnetic moment and the Curie temperature continuously decrease with respect to the undoped composition, as Mn ions are substituted progressively by Co. This is interpreted in terms of substitution of Mn^{3+} by Co^{3+} and the appearance of a small amount of Co^{4+}. The measured magnetoresistance reaches 40 % for the 10 % Co-doped one at the corresponding Curie temperature. The resistivity behaviour of all the studied compounds is determined by the intra- and intergrain conduction mechanisms, with grain sizes in the range of 10–25 nm.

Introduction

Perovskite-like phases with the general formula $Ln^{3+}_{1-x}A^{2+}_xMnO_3$ (Ln^{3+} = La, Pr, Nd, Sm… and A^{2+} = Ca, Sr, Ba, Pb…) have attracted the attention of the scientific community because of the magnetotransport properties exhibited.[1,2] The double exchange mechanism[3] is used to explain the ferromagnetic behaviour of these phases, while the simultaneous presence of ferromagnetism and a metallic state brings about colossal magnetoresistance (CMR) when the magnetic field is changed.[4] These generic magnetic and transport properties in this type of doped manganites mainly arise from a strong on-site exchange interaction (Hund's-rule couple $J \approx 2$–3 eV[5]) between the localised t_{2g} spins and itinerant e_g electrons.[6] The rhombohedral and orthorhombic distortion of the actual crystallographic structure of the classic cubic symmetry is also an essential factor to understand the magnetic and transport properties of these samples.[7]

The substitution of the Mn ions by other transition-metal ions in perovskites of composition $Ln_{0.7}A_{0.3}Mn_{1-y}TM^{3+}_yO_3$ (TM = transition metal) gives rise to changes in the Mn^{3+}:Mn^{4+} ratio, with important modifications in their magnetic and transport properties.[8–12] The $y = 0$ sample shows ferromagnetism and CMR. In this sense, the effect of different trivalent ions from the iron group (partially filled 3d shells) as Fe^{3+} ($3d^5$), Co^{3+} ($3d^6$) or Ni^{3+} ($3d^7$) substitution in the Mn site is still an interesting subject.

We have shown, in previous works,[9,13] that iron enters as high-spin $t_{2g}^3\ e_g^2$ (HS, $S = 5/2$) Fe^{3+} in the $La_{0.7}Pb_{0.3}Mn_{1-x}Fe_xO_3$ family of compositions because it is the most stable oxidation state for this cation, and its ionic radius is very similar to that of the Mn^{3+} ion. Iron couples antiferromagnetically with Mn ions and weakens progressively the double exchange mechanism and so the ferromagnetic character (decrease of both Curie temperature and low-temperature magnetic moment value) of the compounds as the doping level increases. A 20–30% substitution of Fe leads to magnetic frustration and insulating behaviour in these compositions.[13]

The electronic and magnetic properties of the $LaCoO_3$ perovskite is still a matter of research in the scientific community. Goodenough determined that the spin state of the Co^{3+} ions presents a $t_{2g}^6\ e_g^0$ diamagnetic low-spin configuration at low temperatures (LS, $S = 0$), which changes as temperature increases to a $t_{2g}^4\ e_g^2$ high-spin (HS, $S = 2$) state. The possibility of having Co^{3+} in different spin states as a function of temperature arises from the close values of the intra-atomic exchange energy (J_H) and the crystal field splitting (10Dq) at the Co sites. The low-temperature spin state of the Co^{III} ion is due to the large crystal field, which stabilises its low-spin configuration and is energetically

[a] Dpto. de Química Inorgánica, Fac. de Ciencia y Tecnología, Univ. del País Vasco/EHU, Apdo. 644, 48080 Bilbao, Spain
[b] Dpto. de Electricidad y Electrónica-Un. As. CSIC, Fac. de Ciencia y Tecnología, Univ. del País Vasco/EHU, Apdo. 644, 48080 Bilbao, Spain
Fax: +34-94-601-3071
E-mail: jon@we.lc.ehu.es
[c] Institut Laue Langevin (ILL, CRG-D1B), Rue Jules Horowitz, B. P. 156, 38042 Grenoble Cedex 9, France
[‡] New address: Instituto de Ciencia de los Materiales de Aragón, Universidad de Zaragoza, CSIC Facultad de Ciencias, 50009 Zaragoza, Spain

more favourable. Increasing temperature, a thermally activated spin transition from the low-temperature LS state to a paramagnetic HS state occurs; in the range 100–350 K both populations are stabilised in a dynamical equilibrium.[14,15] More recently different authors[16,17] have evidenced the existence of a transition that develops from the low-temperature Co^{3+} (LS, $t_{2g}^6 e_g^0$) to an intermediate spin (occupation $t_{2g}^5 e_g^1$) state, as temperature increases, with energy differences about 10–12 meV between the ground and the first excited state. Also, in Co containing perovskite-like compounds and in particular in cobaltites, the coexistence of those ions with high-spin tetravalent Co^{4+} ($t_{2g}^3 e_g^2$) has also been proposed.

In order to study such a transition and the effect of these different tri- or tetravalent Co cations, we present the results concerning the magnetic and structural properties of the $La_{0.7}Pb_{0.3}(Mn_{1-x}Co_x)O_3$ manganites when Mn is substituted progressively by Co up to 30% doping levels. Similar research work was performed in a family of manganites having Ca instead of Pb occupying the A site.[15] Briefly, it was found that even for small doping levels of Co (as low as $x = 0.05$) the ferromagnetic order of the pure manganite is severely modified. The magnetic-order temperature decreases quickly in the Mn–Co mixed compounds, with almost a constant value of 165–170 K for doping levels ranging from $x = 0.1$ to 0.3. But Ca^{2+} and also Sr^{2+} are cations with ionic character and when cations with a more covalent character, such as Pb^{2+}[13] and Bi^{3+},[18] are used, the observed magnetic behaviour indicates a soft and progressive decrease of the magnetic-order temperatures in each family of compounds.

Neutron diffraction, magnetic and transport measurements have been used in order to perform this study. We have been especially careful in the analysis of the chemical and structural properties of the studied compositions, and tried to explain the observed magnetic and magnetotransport properties on the basis of those previously determined characteristics.

Results and Discussion

The morphology of the $La_{0.7}Pb_{0.3}Mn_{0.9}Co_{0.1}O_3$ compound is shown as representative in the SEM photograph (taken with 8500 times magnification) of Figure 1. The microstructure reveals uniform and fine grain growth, less than 1 μm size, as expected from the sol-gel fabrication process used to synthesise the samples. The observed agglomeration of such fine grains is also a direct consequence of the fabrication process used.

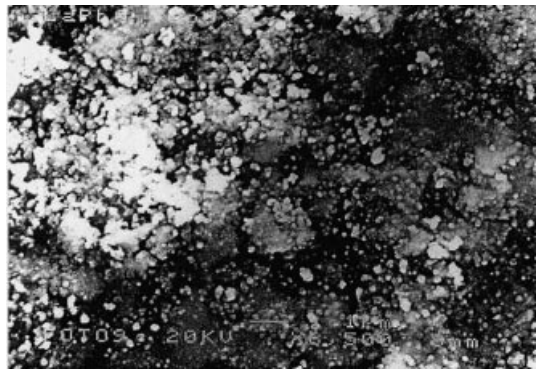

Figure 1. SEM photograph of the $La_{0.7}Pb_{0.3}Mn_{0.9}Co_{0.1}O_3$ compound.

The crystal structure of this family of compounds has been analysed in the trigonal space group ($R\bar{3}c$) (see Figure 2), hexagonal setting ($Z = 6$), using the D1B neutron powder diffraction data.

The Co cation undergoes a spin-state transition, in the range 125–230 K, that is directly correlated with the ionic radius of the cations and is reflected in the thermal evol-

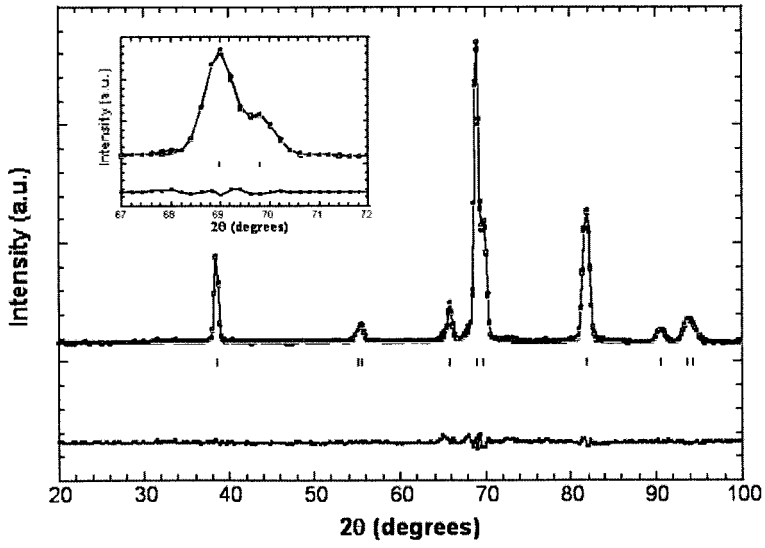

Figure 2. Rietveld fit to the neutron diffraction data (recorded at 10 K) for the $La_{0.7}Pb_{0.3}Mn_{0.7}Co_{0.3}O_3$ compound showing Bragg reflections for the $R\bar{3}c$ phase, difference curve and (inset) refinement of the main diffraction peak, around $2\theta = 69°$.

ution of the Mn/Co–O bond length obtained from the neutron diffraction patterns (see Figure 3). We attribute this transition to be from nonmagnetic (LS) to magnetic intermediate state (IS) of the Co cations, with the appearance of orbital ordering of occupied e_g orbitals, as has been previously observed by other authors in the related compound $LaCoO_3$.[16,17] A very recent work[19] on this subject has proved that Co–O hybridisation has to be taken into account, giving rise to a "covalent" IS, $Co(t_{2g}^5\ e_g^{1.5})$–$O(2p^{5.5})$. However, in our case the Co quantity is small enough to give a precise picture of this transition.

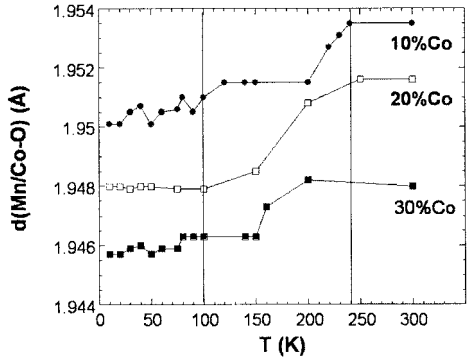

Figure 3. Thermal evolution of the bond length Mn/Co–O for these compounds.

The oxygen stoichiometry of the samples was determined by thermogravimetric analysis, the oxides being heated up to 900 °C in flowing 5% H_2/Ar. The samples were reduced to MnO and CoO and the observed weight losses allowed us to determine the oxygen contents of $La_{0.7}Pb_{0.3}Mn_{0.9}Co_{0.1}O_{3.10}$, $La_{0.7}Pb_{0.3}Mn_{0.8}Co_{0.2}O_{3.17}$ and $La_{0.7}Pb_{0.3}Mn_{0.7}Co_{0.3}O_{3.20}$ for the synthesised samples. The obtained excess of oxygen for all the samples is in good agreement with the quantities obtained from the redox titration, the oxygen excess being a direct consequence of the fabrication process used.

Two losses of consecutive weight based on the temperature for all the samples are observed (see Figure 4). The first loss occurs at a temperature of 437 °C. This temperature increases as the Co doping level in the sample increases, while the second loss happens at approximately the same temperature in all cases.

According to this we can affirm that first the Mn^{4+} and Co^{4+} ions (this one only for the 20% and 30% Co-containing compositions) are reduced to Mn^{3+} and Co^{3+} respectively and when all components appear in the form Mn^{3+} and Co^{3+} (constant amount in all the samples) the second reduction takes place, that is to say, the Mn^{3+} and Co^{3+} ions are reduced to Mn^{2+} and Co^{2+} respectively.

The obtained ZFC–FC curves, for all the compositions, are shown in Figure 5. From ZFC curves, a continuous decrease of the magnetic-order or Curie temperature from 240 K for the 10% Co-doped composition to 180 K for the 30% Co-doped one is clearly observed. This decrease in those magnetic-ordering temperatures can be directly attributed to the progressive suppression of the double exchange

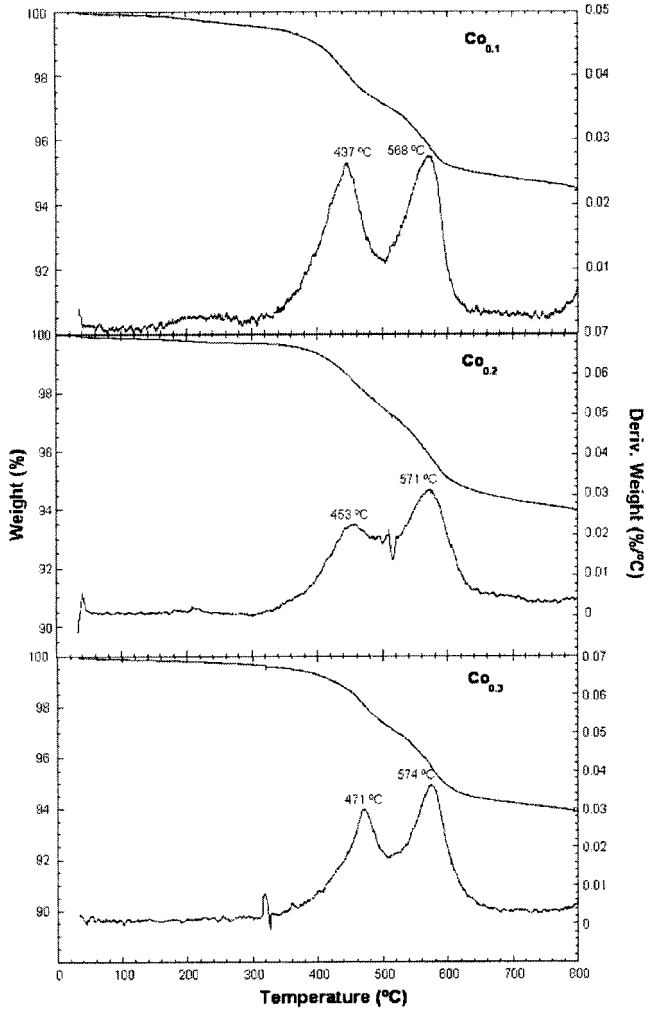

Figure 4. Thermogravimetric curves in H_2. It shows two steps of reduction indicating a reduction process of $TM^{4+} \rightarrow TM^{3+} \rightarrow TM^{2+}$ (TM = Mn and Co).

interaction present in the Mn host as Co content increases in the composition of the samples.

There is a remarkable similarity between this low-field magnetisation behaviour, indicating that the magnetisation process is basically the same. The degree of irreversibility of such processes is high, as indicated by the splitting between ZFC and FC curves. This bifurcation of both curves occurs at a temperature T_b corresponding to the blocking temperature of the largest particles in the assembly. That is, T_b defines also a temperature above which magnetisation processes are fully reversible. It is worth mentioning that the drop of the ZFC magnetisation below T_C for each composition can be interpreted as a feature of cluster glass behaviour. On the other hand, a clear weakening of the ferromagnetic character of these compounds on Co substitution is observed, reflecting a decrease of the measured Curie temperature value as Co content increases in the composition of the samples.

The hysteresis loops, measured at 10 K and up to 7 T (see Figure 6), show the usual ferromagnetic behaviour, quickly reaching magnetic saturation, and the measured values of

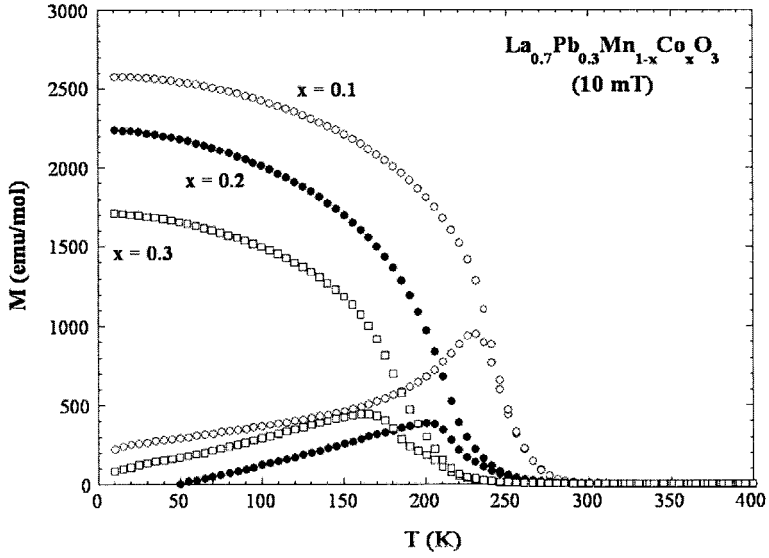

Figure 5. Zero-field cooling (ZFC) and field cooling (FC) curves measured at 10 mT.

the coercive field are 95.5, 114 and 243 kA/m for the 10, 20 and 30% Co-doped compositions, respectively. This high magnitude of the coercive field measured at low temperature can be understood as arising from the strong anisotropic nature of the Co ion.[20] The experimental value of the low-temperature magnetic moment was also determined by using Arrott plots.[21] All measured magnetic data are summarised in Table 1. Previous work from the authors[13] determined the following values for the undoped $La_{0.7}Pb_{0.3}MnO_3$ composition: low temperature $<\mu_{Mn}>_{LT}$ = 3.4 μ_B, T_C = 345 K, high-temperature effective moment $<\mu_{Mn}>_{HT}$ = 5.9 μ_B. For the x = 0.1 composition the measured low-temperature magnetic moment supports our previous supposition that Co enters in the composition only as Co^{3+} (LS) (diamagnetic at low temperatures). However, this is not the case for the x = 0.2 and 0.3 samples. The measured moment values do not agree with the supposition that all Co is Co^{3+}. To account for those measured values (and in particular for the x = 0.2 composition, in which a higher degree of ferromagnetic coupling is observed) we need to assume that also Co^{4+} (HS, S = 5/2) is present in those compositions. In fact, a simple calculation gave us a good fit for the measured low-temperature magnetic moment values taking into account small percentages of about 9% high-spin Co^{4+} for the 20% and 5% for the 30% Co-containing compositions. The existence of Co^{4+} has been observed in other manganite phases.[22] Thus, the low-temperature magnetic properties of these compounds can be understood on the basis of a competition between positive Co^{3+}–O–Co^{4+} and negative Co^{3+}–O–Co^{3+} and Co^{3+}–O–Mn^{4+} interactions, in which it concerns Co ions. Furthermore, a scenario in which Co^{3+} ions cluster around Co^{4+} ions is plausible and justifies the observed zero-field cooled magnetisation behaviour.

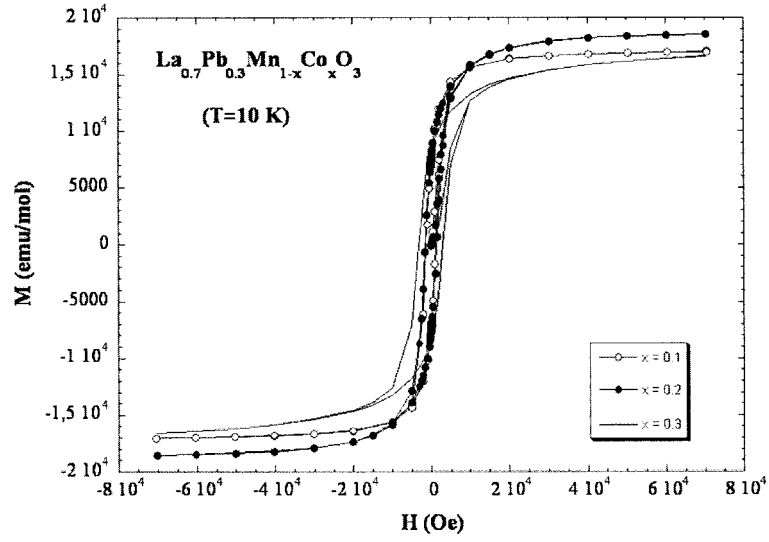

Figure 6. Hysteresis loops measured at 10 K and up to 7 T.

Table 1. Values of the low-temperature magnetic moment and Curie temperature for the $La_{0.7}Pb_{0.3}(Mn_{1-x}Co_x)O_3$ ($0.1 \leq x \leq 0.3$) family of compounds.

Sample	μ [μ_B][a]	μ [μ_B][b]	T_C [K][b]	μ [μ_B][c]	T_{order} [K][c]	μ_{eff} [μ_B][f]	θ_c [K][f]	μ_t [μ_B][g]
Co0.1	3.06	3.05	240	3.04[d]	275	5.31	265	5.6
Co0.2	2.72	3.17	210	2.72[e]	230	5.27	244	5.5
Co0.3	2.38	2.63	180	2.11[e]	190	5.22	230	5.2

[a] Expected values if only Co^{3+} enters in the compositions. [b] Values obtained from magnetic measurements. [c] Values obtained from neutron diffraction. [d] T = 1.5 K. [e] T = 10 K. [f] Values from Curie–Weiss law in the paramagnetic regime. [g] Values calculated as explained in the text.

We can check the validity of this guess by analysing the high-temperature magnetisation behaviour. In Figure 7 we show the $\chi^{-1}_{dc} = H/M_{ZFC}$ versus T behaviour measured in the paramagnetic phase for the different samples. A Curie–Weiss law is clearly followed above T_C and in the temperature range over which the data were taken. The effective moments μ_{eff} obtained from the Curie constants are shown in Table 1, together with the obtained paramagnetic Curie temperatures, θ_C. We have also calculated the expected value μ_t of that effective moment as $\mu_t = [(1 - x)<\mu_{Mn}>^2_{HT} + x<\mu_{Co}>^2]^{1/2}$, taking into account the previous percentages of Co^{4+} (HS) and that only Co^{3+} (covalent IS, 2.5 μ_B[19]) is present for each composition (see Table 1). As expected, all calculated values are slightly higher than the experimental ones, except for the x = 0.3 compound, which shows an excellent agreement between both experimentally determined and calculated values. This sample has the lowest paramagnetic Curie temperature and as a first consequence a better accuracy in the experimental determination of μ_{eff} than the other two compounds because the temperature range used for the fitting extends to temperatures far above T_C.

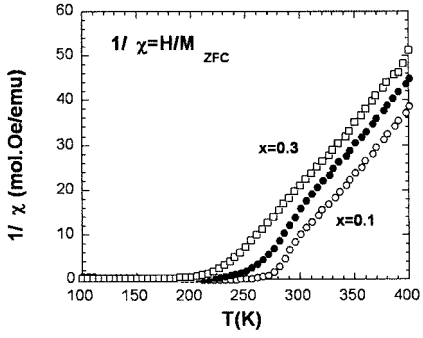

Figure 7. Curie–Weiss plot of the dc susceptibility.

The proposed magnetic behaviour for this family of Co-doped manganites is also supported by our neutron diffraction experiments. The thermal evolution of the neutron diffraction patterns for these samples was also recorded (see Figure 8). In all cases, two reflections with magnetic contribution at the same d values are observed. This feature is indicative of an equivalent magnetic structure for the compounds. That is, the magnetic order does not change its structure when including 10, 20 or 30% of Co in these La-based phases. Furthermore, all magnetic reflections can be indexed with the same cell as the nuclear one, indicating an equivalent type of ferromagnetic structure with collinear magnetic moments. The magnetic contribution appears at about 275, 230 and 190 K for the 10, 20 and 30% Co-doped compositions, respectively. The best solution for the fits was obtained with a collinear magnetic structure in which the magnetic moment of the Mn ion is placed into the (101) crystallographic plane, in the hexagonal setting (parallel to the [111] direction of the perovskite cubic cell) (see Figure 9). The obtained values of the magnetic moment at the lowest temperature of the measurement (1.5 or 10 K) are 2.74, 2.72 and 2.11 μ_B for the 10, 20 and 30% Co-doped compositions, respectively. Figure 10 shows the temperature dependence of the refined magnetic moment value for the studied Co-containing compositions.

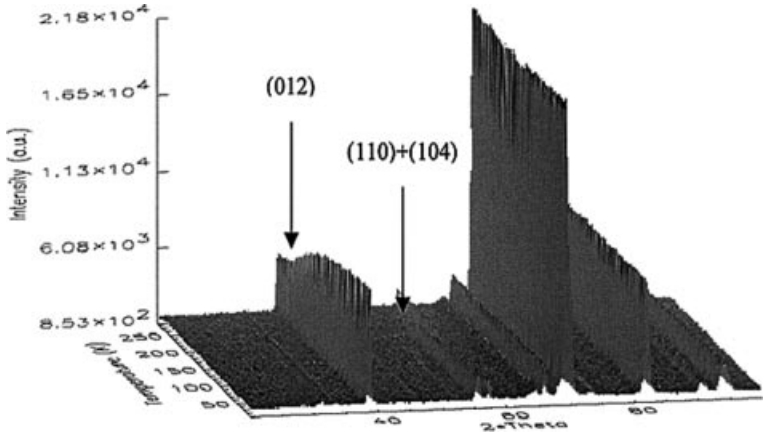

Figure 8. Thermal evolution of the neutron diffraction patterns for the $La_{0.7}Pb_{0.3}Mn_{0.8}Co_{0.2}O_3$ compound.

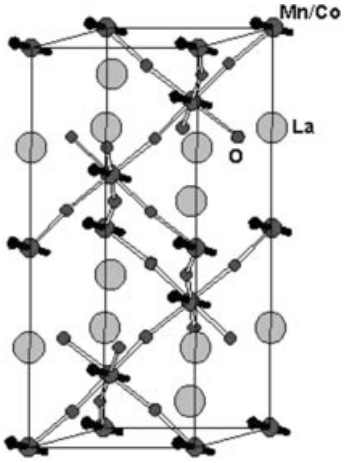

Figure 9. Magnetic structure obtained from neutron diffraction analysis for the $La_{0.7}Pb_{0.3}Mn_{0.8}Co_{0.2}O_3$ compound.

Finally, the room-temperature measured values of the resistivity are 0.098, 0.617 and 0.981 Ω·cm for the 10, 20 and 30% Co-containing samples, respectively. That is, conductivity of the samples decreases as the amount of cobalt that enters into the composition of the samples increases.

From the measured resistivity values as a function of temperature and applied magnetic field we can calculate the magnetoresistance at 6 T as MR (%) = [1 – R(6 T)/R(0 T)] × 100. The magnitude of this magnetoresistance (see Figure 11) is about 25% for the 30% Co-containing sample and reaches 40% for the 10% Co-containing one (with a local maximum arising from an intragrain magnetoresistance mechanism) at the corresponding Curie temperature of each compound. As the doping level of the cobalt increases, a progressive decrease of the MR value is observed (see Table 2).

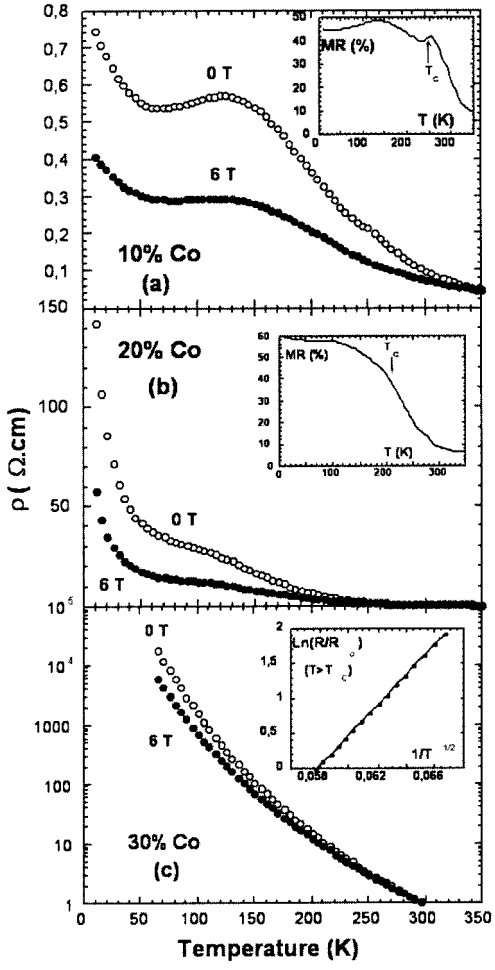

Figure 11. Temperature dependence of the electrical resistivity for all compounds, as the doping level of Co increases. The insets show: (a, b) the corresponding magnetoresistance vs. temperature behaviour and (c) the fit to the VRH mechanism for $T > T_C$.

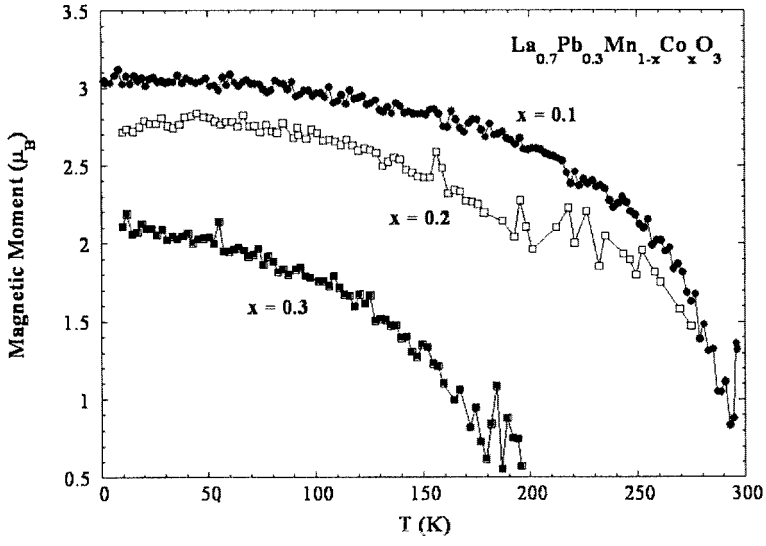

Figure 10. Temperature dependence of the magnetic moment obtained from neutron diffraction data for the Co family of compounds.

It is already well established that the zero-field resistivity data obtained for $T > T_C$ obey the Mott variable range hoping (VRH) mechanism[23] when the carriers are localised near the Fermi energy, as it is in the case of hole-doped manganites. Previous works[24,25] have determined also that the exponent $n = 1/2$ is the most adequate one for this law. Indeed our zero-field resistance data obey Equation (1).

$$\frac{R(T)}{R_0} \propto \exp\left(\frac{T_0}{T}\right)^{1/2} \quad (1)$$

Efros and Shklovskii[26] explained that such resistance behaviour is directly related to a form of hopping favoured by the Coulomb repulsion between carriers. Its most important consequence is the existence of an energy or Coulomb gap, which basically reflects the differences between the minimum energies of adding an electron and subtracting one from the system, without disturbing the other charges. From the obtained T_0 values, we have estimated values for these energy gaps ranging between 1 and 5 eV (see Table 2). In particular, the sample containing 20% of doping element exhibits a gap value higher than that obtained when $Ln_{0.7}A_{0.3}MnO_3$-type perovskites are synthesised by using the ceramic method.[27,28] Other authors have already identified such resistivity behaviour, specially at low temperatures, as arising in samples with low grain size (around 20–30 nm).[29] As previously discussed, our perovskites prepared by the sol-gel method present as one of their characteristics the fine grain obtained,[30] typically below 1 μm (see Figure 1). It is already well established that tunnelling of electric charge into small nanoparticles increases the Coulomb energy by the charging effect, strongly enhancing the tunnel resistance. The grain sizes of our compounds can be roughly estimated by using the measured values of the blocking temperature in ZFC–FC curves. This can be written as $T_b = KV/(25k_B)$, where K is the anisotropy constant and V is the grain volume [$V = (3\pi/4)(d/2)^3$, d being the diameter of the grains, assumed to be spherical for simplicity]. From ferromagnetic resonance experiments in a similar $La_{0.67}Ba_{0.33}MnO_3$ oxide,[31] we used K values in the range $2–4 \times 10^4$ J/m^3. Thus, from the values of $T_b = 215$ K (30% Co, the lowest one) and 255 K (10% Co, the highest one) we infer grain sizes of 10–25 nm for both compositions, in good agreement with the grain sizes obtained from our structural study. But the presence of those nanosized grains in our samples is strongly supported also by the low-temperature behaviour of the resistivity of these compounds.

Table 2. Values of the magnetoresistance at the corresponding Curie temperature and calculated energy gap for the $La_{0.7}Pb_{0.3}(Mn_{1-x}Co_x)O_3$ ($0.1 \le x \le 0.3$) family of compounds.

Sample	ρ_0[a] [Ω·cm]	MR [%]	ΔE [eV][b]
Co0.1	0.098	40	1.9
Co0.2	0.617	38	3.5
Co0.3	0.981	25	4.0

[a] At 300 K and $H = 0$ applied field. [b] Data fitted to the variable range hopping model, $T > T_C$ range.

The resistivity of the 10% Co-doped sample shows typical features of grain boundary (intergrain) effects, that is a maximum of $\rho(T)$ at a temperature well below T_C that is not shifted to higher temperatures by applying an external magnetic field (see Figure 10, a); but at low temperatures and because of the small size of the grains, it is increasingly difficult to activate this intergrain mechanism. In this situation, transport is effectively blocked, giving, as a result, a much higher upturn in the low-temperature resistivity. This is the so-called Coulomb blockade,[32] and appears much more enhanced in the 20% Co-doped composition.

Along this line of reasoning, our experimental data below 100 K fit well to the expression for granular metals [Equation (2)].[33]

$$\rho(T) \approx \exp\sqrt{(\Delta/T)} \quad (2)$$

In Equation (2) Δ is proportional to the activation or charging energy, E_C, of a single grain. From our fits we have obtained values of $\Delta^{1/2} = 2.4$ and 8.5 K$^{1/2}$, and gap energies of 0.5 and 6.2 meV for the Co-10% and Co-20% doped compositions, respectively, that agree with results from other authors[29,34] obtained for related compounds. We also have to mention that the fit to the $T^{-1/2}$ law is better than that to the T^{-1} dependence postulated for a pure Coulomb blockade effect.

Conclusions

In the light of our experimental work, we can conclude that Co enters in the $La_{0.7}Pb_{0.3}Mn_{1-x}Co_xO_3$ family of perovskites, giving rise to low distortion in the structure of these compounds. The measured low-temperature saturation magnetic moments are mainly due to the coexistence of Co^{3+} (LS) and high spin Co^{4+}, as confirmed by susceptibility measurements in the paramagnetic region. The cluster glass behaviour indicated by zero-field cooled magnetisation curves is due to the fact that Co^{3+} probably clusters around Co^{4+} ions. A progressive increase in the doping level of Co gives rise to a subsequent decrease in the measured Curie temperature values, indicating that the long-range ferromagnetism is sensitive even to small amounts of Co.

Because of the sol-gel fabrication process used, we have obtained very homogeneous and small size of the grains (about 10–25 nm as obtained by structural methods and confirmed by magnetic measurements) for all samples. This makes the measured resistivity behaviour to be determined both by the intra- and intergrain carrier tunnelling mechanism that evolve at low temperatures to strong Coulomb blockade for the 20% Co-doped sample.

All compounds show magnetoresistance with magnitudes, at the Curie temperatures, of 40 and 25% for the 10 and 20% Co-doped samples, respectively.

Experimental Section

Mixed oxides of nominal composition $La_{0.7}Pb_{0.3}(Mn_{1-x}Co_x)O_3$ ($0 \le x \le 0.3$) were prepared by the sol-gel method with the required

quantities of analytical grade of La_2O_3, $Pb(NO_3)_2$, $Co(NO_3)_2{\cdot}6H_2O$ and $Mn(C_2H_3O_2)_2{\cdot}4H_2O$ as the starting materials. Citric acid and ethylene glycol were used as gelling agents for the metallic ions in a nitrate solution. After drying in a sand bath for 24 h, the gel obtained was subjected to successive heat treatments at temperatures of 773, 973 and 1073 K, each of 10 h. In order to measure the electrical resistivities of the samples, the powder thus obtained was pelletised with a pressure of 7.2 MPa prior to final sintering at 1173 K for 10 h in flowing oxygen.

The Mn^{3+}/Mn^{4+} content of each sample was determined by redox titration using an excess of $FeSO_4$ solution and back titration with $KMnO_4$. We have observed small deviations from the theoretical stoichiometries that could be due to an excess in the oxygen concentration, in accordance with the preparation method, or more probably to the presence of cation vacancies in the samples. We have obtained a ratio Mn^{3+}/Mn^{4+} of 0.37/0.53 for the $x = 0.1$ compound that changes progressively to 0.10/0.60 for the $x = 0.3$ one. That is, as expected, the Mn^{3+} content decreases as the Co doping level increases in the nominal composition of our samples.

Thermogravimetric measurements were performed in a TA instruments SDT 2960 thermobalance. Approximately 50 mg of sample was placed on an alumina crucible and heated to 900 °C at 5 °C/min in a 5% H_2/Ar current flow.

Scanning electron microscopic (SEM) observations were also performed to give an indication of the compound morphology and compactness using a JEOL JSM-6400 instrument.

The first crystallographic characterisation of the phases was performed by X-ray powder diffraction analysis using a Philips X-Pert diffractometer, working with Cu-K_α1 and Cu-K_α2 radiation, Soller slits of 0.04 rad and receiver and divergence slits of 1°. Powder diffraction patterns were Rietveld fitted using the FULLPROF program.[35]

Magnetic and resistance measurements were conducted in a Quantum Design MPMS-7 SQUID magnetometer. The zero-field cooling (ZFC) and field cooling (FC) curves were performed under an applied field of 10 mT. The order temperature, T_C, was determined from the ZFC curves as the temperature where the minimum of the dM/dT derivative occurs. Hysteresis loops at 10 K and up to 7 T were also obtained. The resistance and magnetoresistance versus temperature measurements were taken by using a conventional dc four-wire system, with the magnetic field applied parallel to the current.

Neutron diffraction measurements were performed at the high-flux reactor at the Institut Laue-Langevin, Grenoble, France. In order to trace the temperature dependence of the structural and magnetic properties, measurements were carried out on D1B. We used a wavelength of 2.519 Å to study the range 2θ = 20–100° at temperatures ranging from 10 to 300 K. The Rietveld analysis of the diffraction data was performed using the FULLPROF program. The line shape of the diffraction peaks was generated by a pseudo-Voigt function and the background interpolated between some fixed background points of the diagrams. In the final run the following parameters were refined: unit-cell parameters, zero-point, half-width, pseudo-Voigt and asymmetric parameters, scale factor, atomic coordinates and thermal isotropic factors. The occupancy factors were also allowed to vary in the last steps of the refinements. Because of the high correlation between the thermal and occupancy factors, in some cases the refinements did not reach the convergence. In those cases, the occupancy factors were fixed to the theoretical ones.

All structural parameters obtained from neutron diffraction experiments together with the tolerance factor (t) of the perovskite structure, $t = (d_{La–O})/\sqrt{2}(d_{Mn/Co–O})$ (with $d_{La–O}$ and $d_{Mn/Co–O}$ the La–O and Mn/Co–O bond lengths), are summarised in Table 3. A previous study of the related parent compound $La_{0.7}Pb_{0.3}MnO_3$ gave as the main structural parameters the following: V = 353.01 Å^3, t = 0.995, Mn–O–Mn = 166.8° and O–Mn–O = 90.71°.[13] We have observed that for our compounds the unit-cell volume decreases with increasing Co content according to the smaller size of this ion. However, this substitution produces only a minor distortion in the MnO_6 octahedra, the O–Mn/Co–O and Mn/Co–O–Mn/Co angles remaining rather constant. The tolerance factor does not suffer any appreciable change for the different compositions. These geometrical characteristics indicate that the distortion of the $La_{0.7}Pb_{0.3}Mn_{1-x}Co_xO_3$ perovskite structure is nearly independent of the x value, in good agreement with the comparable size of Co^{3+} and Mn^{3+} ions. From our structural fits and using the Scherrer formula[36] we have estimated a grain size between 16 and 20 nm.

Table 3. Atomic parameters for the $La_{0.7}Pb_{0.3}(Mn_{1-x}Co_x)O_3$ ($0.1 \leq x \leq 0.3$) family of compounds after the Rietveld refinements of the D1B neutron powder diffraction data. La and Pb atoms are at 6a positions (0, 0, 1/4); Mn and Co atoms are at 6b (0, 0, 0); O atoms are at 18e (x, 0, 1/4). Z = 6 in all cases.

Sample	Co0.1	Co0.2	Co0.3
T [K]	296	280	200
Space group	$R\bar{3}c$	$R\bar{3}c$	$R\bar{3}c$
a [Å]	5.496(2)	5.4948(9)	5.4859(9)
c [Å]	13.346(4)	13.3374(8)	13.2925(9)
V [Å^3]	349.1(2)	348.7(9)	346.4(9)
t	0.995	0.994	0.989
La B[Å^2]/F_{occ}	0.247(3)/0.7	0.247(3)/0.7	0.247(3)/0.7
Pb B[Å^2]/F_{occ}	0.247(3)/0.3	0.247(3)/0.3	0.247(3)/0.3
Mn B[Å^2]/F_{occ}	0.247(3)/0.9	0.247(3)/0.8	0.247(3)/0.7
Co B[Å^2]/F_{occ}	0.247(3)/0.1	0.247(3)/0.2	0.247(3)/0.3
O x	0.4592(1)	0.4565(1)	0.4551(1)
O B[Å^2]/F_{occ}	1.4(4)/0.531	1.4(4)/0.531	1.4(4)/0.531
Mn/Co–O [Å]	1.953(3)x6	1.951(3)x6	1.948(3)x6
La/Pb–O [Å]	2.524(5)x3	2.508(5)x3	2.496(5)x3
	2.741(5)x6	2.741(5)x6	2.734(5)x6
	2.972(6)x3	2.986(6)x3	2.989(6)x3
<La/Pb–O> [Å]	2.7447	2.7443	2.7386
Mn/Co–O–Mn/Co [°]	166.81	165.92	165.48
O–Mn/Co–O [°]	90.7	90.77	90.86
R_p [%]	3.41	4.12	3.64
R_{wp} [%]	4.82	5.79	5.01
χ^2	2.57	3.59	3.00
Bragg R	4.79	4.73	3.89

Acknowledgments

We want to thank the Servicio General de Medidas Magnéticas de la UPV/EHU. We also are grateful to I. de Pedro and to Prof. J. L. Pizarro for their help in magnetic structure discussion. This work has been carried out under projects MAT2002-04178 and MAT2004-2425 of the Spanish Ministerio de Ciencia y Tecnología.

[1] S. Jin, T. H. Tiefel, M. McCormack, R. A. Fastnacht, R. Ramesh, L. H. Chen, *Science* **1994**, *264*, 413.
[2] Y. Tokura (Ed.), *Colossal Magnetoresistive Oxides*, Gordon and Breach Science Publishers, Amsterdam, The Netherlands, **2000**.
[3] C. Zener, *Phys. Rev.* **1951**, *82*, 403–405.
[4] K. Chahara, T. Ohno, M. Kasai, K. Kozono, *Appl. Phys. Lett.* **1993**, *63*, 1990–1992.

[5] Y. Moritomo, A. Machida, K. Matsuda, M. Ichida, A. Nakamura, *Phys. Rev. B* **1997**, *56*, 5088–5091.
[6] P. W. Anderson, H. Hasewaga, *Phys. Rev.* **1995**, *100*, 675–677.
[7] P. G. Radaelli, M. Marezio, H. Y. Hwang, S. W. Cheong, B. Batlogg, *Phys. Rev. B* **1996**, *54*, 8992–8995.
[8] L. Righi, P. Gorria, M. Insausti, J. Gutiérrez, J. M. Barandiarán, *J. Appl. Phys.* **1997**, *81*, 5767–5769.
[9] J. Gutiérrez, J. M. Barandiarán, M. Insausti, L. Lezama, A. Peña, J. J. Blanco, T. Rojo, *J. Appl. Phys.* **1998**, *83*, 7171–7173.
[10] M. Pissas, G. Kallias, E. Devlin, A. Simopoulos, D. Niarchos, *J. Appl. Phys.* **1997**, *81*, 5770–5772.
[11] K. H. Ahn, X. W. Wu, K. Liu, C. L. Chien, *Phys. Rev. B* **1996**, *54*, 15299–15302.
[12] K. Ghosh, S. B. Ogale, R. Ramesh, R. L. Greene, T. Venkatesan, K. M. Gapchup, R. Bathe, S. I. Patil, *Phys. Rev. B* **1999**, *59*, 533–537.
[13] J. Gutiérrez, A. Peña, J. M. Barandiarán, J. L. Pizarro, T. Hernández, L. Lezama, M. Insausti, T. Rojo, *Phys. Rev. B* **2000**, *61*, 9028–9035.
[14] J. B. Goodenough, *J. Phys. Chem. Solids* **1958**, *6*, 287–297.
[15] M. A. Señarís-Rodríguez, J. B. Goodenough, *J. Solid State Chem.* **1995**, *118*, 323–336.
[16] M. A. Korotin, S. Yu. Ezhov, I. V. Solovyev, V. I. Anisimov, D. I. Khomskii, G. A. Sawatzky, *Phys. Rev. B* **1996**, *54*, 5309–5316.
[17] P. Ravindran, H. Fjellvag, A. Kjekshus, P. Blaha, K. Schwarz, J. Luitz, *J. Appl. Phys.* **2002**, *91*, 291–303.
[18] L. Righi, J. Gutiérrez, J. M. Barandiarán, *J. Phys.: Condens. Matter* **1999**, *11*, 2831–2840.
[19] M. Medarde, C. Dallera, M. Grioni, J. Voigt, A. Podlesnyak, E. Pomjakushina, K. Conder, T. Neisius, O. Tjernberg, X. S. N. Barilo, *Phys. Rev. B* **2006**, *73*, 054424-1 to -10.
[20] R. L. Carlin (Ed.), *Magnetochemistry*, Springer, Berlin, Germany, **1986**.
[21] A. Arrott, *Phys. Rev.* **1957**, *108*, 1394–1396.
[22] D. Verma, A. K. Nigam, T. K. Gundu Rao, D. Bahadur, *J. Magn. Magn. Mater.* **2004**, *271*, 172–179, and references therein.
[23] N. F. Mott, *J. Non-Cryst. Solids* **1968**, *1*, 1–17.
[24] J. Gutiérrez, A. Peña, J. M. Barandiarán, J. L. Pizarro, L. Lezama, M. Insausti, T. Rojo, *J. Phys.: Condens. Matter* **2000**, *12*, 10523–10534.
[25] H. Huhtinen, R. Laiho, K. G. Lisunov, V. N. Stamov, V. S. Zakhvalinskii, *J. Magn. Magn. Mater.* **2002**, *238*, 160–167.
[26] A. L. Efros, B. I. Shklovskii, *J. Phys. C: Solid State Phys.* **1975**, *8*, L49.
[27] R. Mahendiran, R. Mahesh, A. K. Raychaudhuri, C. N. R. Rao, *Solid State Commun.* **1995**, *94*, 515–518.
[28] H. Song, W. J. Kim, S.-J. Kwon, *J. Magn. Magn. Mater.* **2000**, *213*, 126–134.
[29] L. Balcells, J. Fontcuberta, B. Martínez, X. Obradors, *Phys. Rev. B: Condens. Matter* **1998**, *58*, R14697–R14700.
[30] A. Peña, J. Gutiérrez, J. M. Barandiarán, J. P. Chapman, M. Insausti, T. Rojo, *J. Solid State Chem.* **2003**, *174*, 52–59.
[31] S. E. Lofland, S. M. Bhagat, H. L. Ju, G. C. Xiong, T. Venkatesan, R. L. Greene, *Phys. Rev. B: Condens. Matter* **1995**, *52*, 15058–15061.
[32] M. García-Hernández, F. Guinea, A. de Andrés, J. L. Martínez, C. Prieto, L. Vázquez, *Phys. Rev. B: Condens. Matter* **2000**, *61*, 9549–9552.
[33] P. Sheng, *Philos. Mag. B* **1992**, *65*, 357.
[34] J. M. D. Coey, A. E. Berkowitz, L. Balcells, F. F. Putris, A. Barry, *Phys. Rev. Lett.* **1998**, *80*, 3815–3818.
[35] J. Rodríguez-Carvajal, computer code FULLPROF, Rietveld Pattern Matching Analysis of Powder Patterns, ILL, Grenoble, **1990**.
[36] B. E. Warren (Ed.), *X-ray Diffraction: Diffraction by Imperfect Crystals*, Dover Publications, Inc., New York, USA, **1969**.

Received: February 6, 2006
Published Online: June 14, 2006

